Institut Lavoisier – IREM – Université de Versailles
78035 VERSAILLES cedex – France

Dr. Anne Dolbecq (dolbecq@chimie.uvsq.fr, 01 39 25 43 83, fax 01 39 25 43 81)

Versailles, June 12th, 2007

Dear Editor,

Please find our manuscript "Fe_2 and Fe_4 Clusters Encapsulated in Vacant Polyoxotungstates: Hydrothermal Synthesis, Magnetic, Electrochemical Properties, and DFT calculations" that we submit as a full paper to *Chemistry, a European Journal*.

In this paper, we report:

i) The characterization of an unique asymmetric dibridged dinuclear Fe(III) complex, where one metal center is embedded in an inorganic ligand while the other is connected to organic ligands. The value of the exchange coupling parameter between the two paramagnetic centers has been experimentally quantified and found surprisingly low. This result has been rationalized using DFT calculations.

ii) The first butterfly-like polyoxometalate complex, which can be seen as the condensation product of two units similar to the dinuclear complex mentioned above. The physical properties of this compound have been compared to that found for previously reported organic ligand / Fe(III) butterfly systems.

iii) A purely inorganic dinuclear Fe(III) polyoxometalate, where the two iron centers are very strongly magnetically coupled.

The electrochemical properties of the hybrid species have been studied in the solid state and also in solution in the case of the soluble hybrid dinuclear compound.

In all cases, the magnetic exchange coupling interactions have been determined. On a synthetic point of view, this study shows that monovacant polyoxometalates (POMs) can be used as precursors for the synthesis under hydrothermal conditions of magnetic polynuclear clusters with POMs ligands. Such species cannot be isolated under usual bench conditions. This work opens the way to the synthesis of a great variety of compounds by varying the nature of the POM, the transition metal, and the ligand.

Sincerely yours,

Anne Dolbecq

Fe_2 and Fe_4 Clusters Encapsulated in Vacant Polyoxotungstates: Hydrothermal Synthesis, Magnetic, Electrochemical Properties, and DFT calculations

Céline Pichon,[a] Anne Dolbecq,*[a] Pierre Mialane,[a] Jérôme Marrot,[a] Eric Rivière,[b] Monika Goral,[c] Monika Zynek, [c] Timothy McCormac,[c] Serguei A. Borshch,[d] Ekaterina Zueva,[e] and Francis Sécheresse[a]

[a] C. Pichon, Dr. A. Dolbecq, Dr. P. Mialane, Dr. J. Marrot, Prof. F. Sécheresse
Institut Lavoisier, IREM, UMR 8180,
Université de Versailles Saint-Quentin en Yvelines
45 Avenue des Etats-Unis, 78035 Versailles cedex (France)
E-mail: dolbecq@chimie.uvsq.fr

[b] Dr. E. Rivière
Institut de Chimie Moléculaire et des Matériaux d'Orsay
UMR 8182, Equipe Chimie Inorganique
Univ Paris-Sud, 91405 Orsay (France)

[c] M. Goral, M. Zynek, Dr. T. McCormac
Centre for Research in Electroanalytical Technology 'CREATE', Institute of Technology Tallaght, Department of Science, Dublin 24 (Ireland)

[d] Dr. S. Borshch

Laboratoire de Chimie, UMR 5182,

Ecole Normale Supérieure de Lyon,

46 Allée d’Italie, 69364 Lyon Cedex 07 (France)

[e] Dr. E. Zueva

Department of Inorganic Chemistry,

Kazan State Technological University,

Kazan, 420015 (Russia)

Abstract

While the reaction of $[PW_{11}O_{39}]^{7-}$ towards first row transition metal ions M^{n+} under usual bench conditions only leads to monosubstituted $\{PW_{11}O_{39}M(H_2O)\}$ anions, we show that the use of this precursor under hydrothermal conditions allows to isolate a family of novel polynuclear molecular magnetic polyoxometalates (POMs). The hybrid asymmetric $[Fe^{II}(bpy)_3][PW_{11}O_{39}Fe_2^{III}(OH)(bpy)_2]\cdot 12H_2O$ complex (**1**) contains the dinuclear $\{Fe(\mu\text{-}O(W))(\mu\text{-}OH)Fe\}$ core where one iron atom is coordinated to a monovacant POM while the other is coordinated to two bipyridine ligands. Magnetic measurements indicate that in **1** the Fe^{III} centers are weakly antiferromagnetically coupled (J = -11.2 cm^{-1}, $\hat{H} = -J\hat{S}_1\hat{S}_2$) compared to $\{Fe(\mu\text{-}O)(\mu\text{-}OH)Fe\}$ systems. This is due to the long distance between the iron center embedded in the POM and the oxygen atom of the POM bridging the two magnetic centers but also, as shown by DFT calculations, to the important mixing of bridging oxygen orbitals with orbitals of the POM tungsten atoms. $(Hdmbpy)_2[Fe^{II}(dmbpy)_3]_2[(PW_{11}O_{39})_2Fe_4^{III}O_2(dmbpy)_4]\cdot 14H_2O$ (**2**) (dmby = 5,5′-dimethyl-2,2′-bpy) and $H_2[Fe^{II}(dmbpy)_3]_2[(PW_{11}O_{39})_2Fe_4^{III}O_2(dmbpy)_4]\cdot 10H_2O$ (**3**) represent the first butterfly-like POM complexes. In these species, a tetranuclear Fe^{III} complex is sandwiched between two lacunary polyoxotungstates which are pentacoordinated to two Fe^{III} cations, the remaining paramagnetic centers being each

coordinated to two dmbpy ligands. The best fit of the $\chi_M T$ = f(T) curve leads to J_{wb} = -59.6 cm^{-1} and J_{bb} = -10.2 cm^{-1} ($\hat{H}$ = -$J_{wb}(\hat{S}_1\hat{S}_2 + \hat{S}_1\hat{S}_{2*} + \hat{S}_{1*}\hat{S}_2 + \hat{S}_{1*}\hat{S}_{2*}) - J_{bb}(\hat{S}_2\hat{S}_{2*}))$. While the J_{bb} value is within the range of related exchange parameter previously reported for non-POM butterfly systems, the J_{wb} constant is significantly lower. As for complex **1**, this can be justified considering Fe_w-O distances. Finally, in absence of coordinating ligand, the dimeric complex $\mathbf{[N(CH_3)_4]_{10}}[(PW_{11}O_{39}Fe^{III})_2O]\cdot 12H_2O$ (**4**) has been isolated. In this complex, the two single oxo-bridged Fe^{III} centers are very strongly antiferromagnetically coupled (J = -211.7 cm^{-1}, $\hat{H}$ = -$J\hat{S}_1\hat{S}_2$). The electrochemical behavior of compound **1** both in DMSO solution and in the solid state is also presented, while the electrochemical properties of **2**, which is insoluble in common solvents, have been studied in the solid state.

Keywords: density functional calculations · hydrothermal synthesis · magnetic properties · polyoxometalates · solution and solid state electrochemistry

Introduction

Most of the polyoxometalates (POMs) architectures are based on specific structural types, such as the Lindquist (e.g. $[W_6O_{19}]^{2-}$), Keggin (e. g. $[PW_{12}O_{40}]^{3-}$) or Dawson (e. g. $[P_2W_{18}O_{62}]^{6-}$)[1] although POMs with new topological arrangements are still discovered.[2] Lacunary polyoxotungstates act as ligands which can bind to 3d transition metal ions giving rise to species containing transition metal clusters with nuclearities from 1 to 27,[3] exhibiting appealing properties particularly in the field of molecular magnetism[4] and catalysis.[5] Furthermore, the incorporation of exogeneous ligands bridging the paramagnetic centers allows to modulate the magnetic coupling between the transition metal ions encapsulated within the POM.[6] Most of these POMs compounds are synthesized by the direct reaction of the lacunary precursor with transition metal ions under mild conditions (ambient pressure, T < 100°C). The use of hydrothermal conditions with preformed POMs as precursors has been limited so far mainly to saturated Keggin anions such as $[SiW_{12}O_{40}]^{4-}$, leading to materials with isolated transition metal ions.[7] A rare example of vacant POM introduced in a hydrothermal reactor, $[SiW_{10}O_{36}]^{8-}$, has led to the neutral molecular complex $\{Cu_2(O_2CMe)_2$(5,5′-dimethyl-2,2′-bipy$)_2\}$\{Cu(5,5′-dimethyl-2,2′-bipy)2\}$[SiW_{12}O_{40}]$ because of the instability of the lacunary precursor.[8] It is only very recently that the first example of the successful use of lacunary POMs as precursors (i.e. with conservation of the introduced lacunary POM ligand) has been reported, affording monomeric hexanuclear clusters.[9] On another hand, numerous structures of polyoxotungstates synthesized with Na_2WO_4 as

precursor under hydrothermal conditions have been described these last years, giving access to materials based on isopolyoxotungstates,[10] phosphotungstates,[10b,11] germanotungstates[12] or silicotungstates[10b,11d,13] building units, according to the presence or absence of heteroelement. It must be noted that when tungstate is used as precursor in such conditions, it is so far difficult, if possible at all, to control the nature of the resulting POM ligand. Moreover, in most of the cases, saturated POM systems are obtained. Concerning the nature of the 3d transition metal used, numerous heteropolyoxotungstate based materials incorporate copper ions. This can be related to the Jahn-Teller effect in Cu^{II} complexes which permits diverse connecting modes between the POMs and the 3d center. On the contrary, to our knowledge, only one example of iron containing POM system synthesized under hydrothermal conditions, a $[PW_{12}O_{40}]^{3-}$ anion decorated by a $\{Fe^{II}(phen)_2(H_2O)\}$ group, has been reported,[14] while the synthesis of iron based POM materials has been largely explored in usual bench conditions. These multi-iron complexes exhibit spectacular structures,[3] and appealing magnetic[15] or electrochemical properties[16] but their interest lie also in their catalytic properties,[17] biomimetic catalysis being sometimes invoked. Indeed, POMs can be seen as rigid polydentate ligands with electron-acceptor properties, featuring the active site of natural enzymes.[18]

We have thus decided to explore the reactivity of preformed vacant POMs with iron(III) ions under hydrothermal conditions and we report our first results with monolacunary $[PW_{11}O_{39}]^{7-}$ anions as building units in presence or in absence

of organic ligands. A unique asymmetric dibridged dinuclear Fe^{III} complex, where one metal center is embedded in a $[PW_{11}O_{39}]^{7-}$ unit while the other is connected to bipyridine ligands, has been characterized. The value of the exchange coupling parameter between the two paramagnetic centers has been experimentally quantified and found surprisingly low. This result has been rationalized using DFT calculations. The first butterfly-like POM complex, which can be seen as the condensation product of two units similar to the dinuclear complex mentioned above, has also been obtained. The magnetic properties of this compound have been compared to that found for previously reported organic ligand / Fe^{III} butterfly systems. Finally, in absence of organic ligand, a purely inorganic dinuclear Fe^{III} polyoxometalate, where the two iron centers are very strongly antiferromagnetically coupled, has been characterized. The electrochemical properties of the hybrid species are also reported.

Results and Discussion

Syntheses, IR spectroscopy and TG analysis: Dark red crystals of $[Fe^{II}(bpy)_3][PW_{11}O_{39}Fe_2^{III}(OH)(bpy)_2]\cdot 12H_2O$ (**1**) have been obtained in high yield by the reaction of $[\alpha\text{-}PW_{11}O_{39}]^{7-}$, $Fe_2(SO_4)_3$ and 2,2′-bpy with the ratio 1 : 1.5 : 5 in water at 160°C. A slight modification on the organic ligand has led to a dimerization of the anionic unit. $(Hdmbpy)_2[Fe^{II}(dmbpy)_3]_2[(PW_{11}O_{39})_2Fe_4^{III}O_2(dmbpy)_4]\cdot 14H_2O$ (**2**) has

thus been isolated in conditions similar to **1** except that 5,5′-dimethyl-2,2′-bpy (dmbpy) has been used instead of 2,2′-bpy. When the quantity of organic ligand is lowered, other parameters remaining unchanged, only the nature of the counter-cations is modified, two protons replacing two protonated $Hdmbpy^{+}$ cations to lead to $H_2[Fe^{II}(dmbpy)_3]_2[(PW_{11}O_{39})_2Fe_4^{III}O_2(dmbpy)_4]\cdot 10H_2O$ (**3**). Finally, when non-coordinating tetramethylammonium cations are introduced in the synthetic medium in place of the chelating bpy ligands, the dimeric compound $[N(CH_3)_4]_{10}[(PW_{11}O_{39}Fe^{III})_2O]\cdot 12H_2O$ (**4**) crystallizes.

1–**4** are only obtained in a limited pH domain around 3. When the pH is too low, the monovacant POM is unstable and gives the saturated $[PW_{12}O_{40}]^{3-}$ anion. Preliminary X-ray diffraction studies[19] suggest that the crystals isolated with the experimental conditions used for **2**, except that the initial pH was 2, contain $[PW_{12}O_{40}]^{3-}$ anions and $[Fe^{II}(dmbpy)_3]^{2+}$ counter-ions. At higher pH the yield and the crystallinity of **1**–**4** are lowered. Furthermore it can be noticed that **1** was first obtained by the reaction of $[A\text{-}\alpha\text{–}PW_9O_{34}]^{9-}$, showing the instability of this precursor under such conditions. **1** and **4** are slightly soluble in DMSO while **2** and **3** are totally insoluble in common solvents.

The infrared spectra of **1**–**4** have been recorded between 4000 and 400 cm^{-1}. **2** and **3** differing only by the presence of protons have almost identical infrared spectra while the

spectra of **1**, **2** and **4** exhibit slight differences in the 1100-400 cm^{-1} region (Figure SI1, Supporting Information). The splitting ($\Delta\nu$) of the asymmetric P-O stretching vibration of the distorted central PO_4 tetrahedron is thus more pronounced in **4** (1093, 1057, $\Delta\nu = 36$ cm^{-1}) than in **2** (1084, 1064, $\Delta\nu = 20$ cm^{-1}) and in **1** (1075, 1066, $\Delta\nu = 9$ cm^{-1}). It is usually admitted that the splitting of the asymmetric P-O stretching vibration in a monosubstituted $\{PW_{11}M\}$ anion is related to the strength of the M-O(PO_3) bond. The splitting is thus maximal for M = Cu^{II} (1105, 1065, $\Delta\nu = 40\ cm^{-1}$) and closest to the splitting observed in $[PW_{11}O_{39}]^{7-}$ (1085, 1040, $\Delta\nu = 45$ cm^{-1}).[20] The splitting in **4** is thus close to the largest splittings observed in the family of monosubstituted lacunary derivatives while the splitting in **2** is more in the order of the values reported for $[PW_{11}O_{39}(H_2O)Fe^{III}]^{4-}$ (1084, 1060, $\Delta\nu = 24$ cm^{-1})[21] and the splitting in **1** tends to the zero splitting value of the saturated $[PW_{12}O_{40}]^{3-}$ anion. The increasing value of $\Delta\nu$ from **1** to **4** can then be tentatively explained by weaker interactions between the metal and the POM as shown by the significant elongation of the Fe-O(PO_3) bond from **1** to **4** (Table 1, see also structural description below).

Thermogravimetric analysis (TGA) was performed, showing similar behaviors for the four compounds (Figure SI2 Supporting Information) and confirming i) the number of hydration water molecules and ii) the number of bpy ligands of **1**-**3** and of TMA^+

counter-ions for 4. The first loss corresponds to the departure of water molecules. For **1–3** on further heating a two-steps weight loss is observed between 300 and 800°C with a total weight loss corresponding to the departure of the bpy molecules. The two-steps departure of 2,2′-bpy ligands has already been observed and attributed to the retention of carbon from the calcination of bpy, the carbon being only slowly removed from the solid residue.[22]

Structural analysis: **1-3** are molecular compounds with substituted POMs anions and monomeric iron complexes bound to bpy ligands as counter-cations. Although the iron precursor contains Fe^{III} ions, it is doubtless that the cations are low spin $[Fe^{II}(bpy)_3]^{2+}$ complexes for three main reasons: i) to the best of our knowledge $[Fe^{III}(bpy)_3]^{3+}$ complexes have been very rarely reported due to the greater stabilization of the +II oxydation state of the metal center by bpy ligands,[23] ii) the charge of the counter-cations is consistent with the results of elemental analyses and electroneutrality considerations, iii) magnetic measurements indicate that for **1-3** the counter- ions are diamagnetic (see below). However the nature of the reducing agent of the Fe^{III} ions is not elucidated.

In **1** the anion (Figure 1) can be described as a dissymmetric dinuclear Fe_2 complex, the Fe(1) ion is bound to the pentadentate monolacunary $[PW_{11}O_{39}]^{7-}$ anion while the Fe(2) ion is linked to two 2,2′-bpy ligands. Fe(1) and Fe(2) are bridged by two oxygen atoms, O(7) being a O=W atom of the POM ligand and O(9) belonging to a hydroxo ligand as indicated by valence bond calculations (Σs = 1.23).[24] Valence bond

calculations also confirm the valence of Fe(1) (Σs = 3.11) but it should be noted that these calculations are not conclusive for ions bound to bpy ligands. The $Fe(1)O_6$ octahedron is highly distorted in the equatorial plane with the Fe(1)-O(7) distance far longer than the three other Fe-O distances but also axially, the Fe-O(PO_3) distance being elongated (Table 1).

As the anion is common in the structures of **2** and **3**, its description will only be given for **2**. This anion (Figure 2a) can be viewed as the condensation of two anions present in **1**. Considering the labels used for compound **1** (Figure 1), this condensation can be seen as resulting from the breaking of the Fe(2)-O(7) bond and the concomitant formation of a Fe(2)-O(9) bound with a neighboring anion. The tetranuclear Fe_4 complex encapsulated between the two POMs belongs to the well-known family of the butterfly complexes.[25] The Fe(2)-Fe(2)* fragment (Figure 2b) features the body of the butterfly while the Fe(2)-Fe(1)-Fe(2)* and Fe(2)-Fe(1)*-Fe(2)* triangles schematize the wings, the Fe(1) and Fe(1)* ions thus occupying the “wingtip” positions. The dihedral angle between the least-squares planes defined by the Fe(1)/Fe(2)/Fe(2)* and Fe(1)*/Fe(2)/Fe(2)* ions is 175.5°, thus the four Fe^{III} ions are essentially coplanar. The sum of the Fe-O-Fe angles around the μ_3-O O(40) atom is equal to the ideal value of 360°. Valence bond calculations indicate that O(40) (Σs = 1.88) is an oxo ligand and confirm the valence of Fe(1) (Σs = 2.97). The $Fe(1)O_6$ octahedron is more axially distorted in **2** than in **1** (Table 1), i.e. the interaction of the Fe(1) ion with the monolacunary POM is

weaker in **2** than in **1** which is expressed in the infrared spectra (see above).

In **4**, the anion results from the dimerization of two $[PW_{11}O_{39}Fe^{III}(H_2O)]^{4-}$ anions (Figure 3). In the dimer the Fe^{III} centers encapsulated in the vacant POMs are bridged by a single oxo ligand as indicated by valence bond calculations (Σs = 1.94), which also confirm the +III oxidation state of the metallic centers (Σs = 3.12 for Fe(1) and 3.23 for Fe(2)). The dimerization of $[PW_{11}O_{39}Fe^{III}(H_2O)]^{4-}$ leading to $[\{PW_{11}O_{39}Fe^{III}\}_2O]^{10-}$ has been previously evidenced in aqueous solution but it had not been possible to isolate and characterize the dimer in the solid state.[26] The dimerization of transition metal mono-substituted POMs has also been studied for titanium (in organic medium),[27] zirconium[28] and ruthenium[29] derivatives but the structural characterization of a μ-oxo bridged dimer has only been very recently performed in the case of $[\{SiW_{11}O_{39}Ru^{IV}\}_2O]^{10-}$.[29b] As observed in this latter compound the dimeric anion in **1** does not possess any symmetry element. The axial distortion of the FeO_6 octahedra in **4** is still higher than that observed in **2** (Table 1). The Fe^{III}-O-Fe^{III} angle (165°) is larger than the Ru^{IV}-O-Ru^{IV} bridging angle (154°) in $[\{SiW_{11}O_{39}Ru^{IV}\}_2O]^{10-}$.

Magnetic properties: The magnetic behaviour of **1** was investigated between 2 and 300 K and is shown under the form $\chi_M T$ versus T (Figure 4), χ_M being the magnetic susceptibility for one mole of **1**. The $\chi_M T$ value at room temperature (7.30 cm^3 mol^{-1} K) is already lower than the calculated $\chi_M T$ value of 8.75 cm^3 mol^{-1} K for two non interacting high spin Fe^{III} centers with

g = 2.00. The $\chi_M T$ curve continuously decreases upon sample cooling, reaching a $\chi_M T$ value of 0.40 cm^3 mol^{-1} K at 2 K. This behaviour is characteristic of an antiferromagnetic interaction with a diamagnetic ground state. The $\chi_M T$ curve was fitted with the Bleaney-Bowers equation deriving from the HDVV Hamiltonian $\hat{H} = -J\hat{S}_1\hat{S}_2$ with $S_1 = S_2 = 5/2$ associated to the two interacting Fe^{III} centers within the dinuclear cluster. The best fit parameter obtained is J = -11.2 cm^{-1} and g = 1.98 (R = 4.8 10^{-6}).[30] Dinuclear iron complexes with oxo, hydroxo, peroxo or carboxylato bridges continue to attract much attention, mainly as models of metalloenzymes, and their magnetic properties have been widely studied.[31] Diferric complexes with $Fe^{III}(\mu\text{-}O)(\mu\text{-}OH)Fe^{III}$ cores are antiferromagnetically coupled with a J value around -100 cm^{-1},[32] far larger than the value determined in **1**. The J value in **1** is thus more in the order of the J values observed for dibridged diferric complexes with one μ-OH ligand, the second bridge being an hydroxo, an alkoxo or a phenolato ligand.[31a] The present result confirms that the exchange interactions mediated through oxygen atoms connected to tungsten centers are very weak, and *a fortiori* much weaker than those commonly observed in μ-O bridged compounds. Focusing on iron systems, it has been shown that for supported[33] and unsupported[34] oxo bridged compounds the Fe-O distance is the main parameter which governs the strength of the magnetic interaction. In **1**,

the Fe-(μ–O(POM)) distances are long (1.915(11) and 2.106(11) Å) compared to those classically found in dinuclear μ-O bridged Fe^{III} complexes, which justifies the low *J* value determined for this compound. DFT calculations on **1** have been performed in order to clarify this point (see below).

As the magnetic cluster in **2** and **3** are similar, the magnetic data have been recorded only on a sample of **2**. The $\chi_M T$ value at room temperature (4.3 cm^3 mol^{-1} K) is far lower than the calculated $\chi_M T$ value of 17.5 cm^3 mol^{-1} K for four non interacting high spin Fe^{III} centers (assuming g = 2.00), indicating relatively strong antiferromagnetic interactions (Figure 5). This is also shown by the continuous decrease of the $\chi_M T$ curve upon sample cooling. As already mentioned the Fe_4 core in **2** belongs to the well known class of butterfly complexes. In these compounds, a rigorous interpretation would imply to consider three *J* values: J_{wb} between one body iron and one external atom, J_{ww} between the two wingtip iron atoms and J_{bb} between the two body iron atoms (Figure 2c). However, considering that the J_{wb} exchange parameter must be weaker than J_{bb} and J_{ww} due to the long Fe(1)···Fe(1) distance, only J_{bb} and J_{ww} are usually considered. This also avoids overparametrization. The corresponding Hamiltonian for this model can thus be expressed as:

$$\hat{H} = -J_{wb}(\hat{S}_1\hat{S}_2 + \hat{S}_1\hat{S}_{2*} + \hat{S}_{1*}\hat{S}_2 + \hat{S}_{1*}\hat{S}_{2*}) - J_{bb}(\hat{S}_2\hat{S}_{2*})$$

with $S_1 = S_2 = S_{1*} = S_{2*} = 5/2$. A best fit of the experimental $\chi_M T$ curve gave $J_{wb} = -59.6$ cm^{-1} and $J_{bb} = -10.2$ cm^{-1}, assuming g = 2.00 (R = 6.31 10^{-5}).[30] As usually observed, the J_{wb} coupling constant is antiferromagnetic and corresponds to the strongest interaction.[35] Compared to other butterfly compounds,[35] this value is the smallest observed value ($-92.0 \leq J_{wb} \leq -65.7$ cm^{-1}), and this can be again correlated to long Fe_w-O distances (1.93 Å in **2**, $1.81 \leq Fe_w\text{-}O \leq 1.89$ Å in compounds reported in the literature), Fe_w being the iron center of the wing. The J_{bb} coupling constant is weakly antiferromagnetic but it should be noted that similarly satisfactory fits could be obtained for $-12 < J_{bb} < -8$ cm^{-1}, as shown by the error contour plot in Figure 6. On the other hand only values of J_{wb} close to -59.6 cm^{-1} give low R values (Figure 6). This lack of definition of J_{bb} has already been discussed and has been related to spin frustration of the centered spins.[25a,25b,25c] The J_{bb} value is in the range of the previously reported values ($-21.8 \leq J_{bb} \leq -2.4$ cm^{-1}) but its absolute value is significantly lower than that found for the recently reported compound $[Fe_4O_2Cl_2(O_2CMe)\{(py)_2CNO\}_4]$ ($(py)_2CNO$ = di-2-pyridyl ketone oxime, $J_{bb} = -59.4$ cm^{-1})[25d] which possesses a triplet ground state, thus confirming that the ground state in **2** is diamagnetic.

As expected for a Fe-O-Fe dimer, the two Fe^{III} centers are strongly antiferromagnetically coupled in **4** as shown (Figure

7) by i) the low $\chi_M T$ value at room temperature (0.85 cm^3 mol^{-1} K) which is more than ten times lower than the calculated $\chi_M T$ value of 8.75 cm^3 mol^{-1} K for two non interacting high spin Fe^{III} centers (assuming g = 2.00) and ii) the strong J value of -211.7 cm^{-1} determined by fitting the $\chi_M T$ curve with the Bleaney-Bowers equation deriving from the HDVV Hamiltonian $\hat{H} = -J\hat{S}_1\hat{S}_2$ with $S_1 = S_2 = 5/2$, assuming g = 2.00 ($R = 4\ 10^{-5}$). The J value in **4** falls in the range of the J values determined for single oxo-bridged diiron(III) complexes ($-240 < J < -160$ cm^{-1}),[31] confirming the protonation degree of the oxygen atom connecting the two $\{PW_{11}O_{39}Fe^{III}\}$ sub-units.

DFT calculations: The DFT calculations of the exchange parameter for the cluster **1**, containing two paramagnetic Fe^{III} centers were performed with the goal to determine the role of different structural and electronic factors. Firstly, the calculations were done for the cluster **1** at the experimentally found geometry. As usually in the broken-symmetry DFT method two states were calculated, namely the high-spin (HS) state with the total spin S = 5 and the broken-symmetry (BS) state, and the exchange parameter was estimated through the expression derived by Yamaguchi $J = 2(E_{BS}-E_{HS})/(\langle S^2\rangle_{HS}-\langle S^2\rangle_{BS})$. We obtained J = -12 cm^{-1}, which is very close to the experimentally observed value -11.2 cm^{-1}. In order to compare this case with the situation in di-iron(III) complexes with one μ-oxo and one μ-hydroxo bridges we also performed

calculations for the model dinuclear complex $[Fe_2^{III}(\mu\text{-}O)(\mu\text{-}OH)(bpy)_4]^{3+}$. The structure of the model complex was optimized for its HS state. The calculations again led to an antiferromagnetic interaction between Fe^{III} ions with J = -68 cm^{-1}, which is much stronger than for the polyoxometalate encapsulated dimer. Nevertheless, this value corresponds more to the range characteristic for dibridged iron complexes (see above). The main reasons for such a difference can be looked for in the geometry of the $\{Fe_2^{III}(\mu\text{-}O)(\mu\text{-}OH)\}$ core. Due to the bond with the polyoxometalate tungsten atom, the bridging oxygen atom in **1** is well separated from the Fe(1) atom (2.106 Å), and the distance to Fe(2) is equal to 1.915 Å. In the symmetric model complex both distances are equal to 1.90 Å. Different hypotheses can be found in the literature concerning magnetostructural correlations in oxo-bridged iron(III) dimers. In some works J values for asymmetric complexes was correlated with the mean Fe-O distance,[33] whereas the correlation with the longest Fe-O distance was also proposed.[36] But in any case, the changes in the geometry of the Fe-O-Fe linking between the model complex and **1** must lead to a weakening of the magnetic interaction. Another factor, which can be also responsible for the variation of exchange coupling, is the important mixing of magnetic orbitals, composed of 3d iron orbitals with participation of 2p bridging oxygen orbitals, with 5d orbitals of polyoxometalate tungsten

atoms linked to μ-oxo bridges. The latter enter into the magnetic orbitals with about the same weight as iron orbitals. This situation differs from the earlier considered case of diiron substituted γ-Keggin silicotungstates,[37] where magnetic orbitals are only slightly mixed with tungsten orbitals (see Fig.6 and Table 7 in Ref. 37) and the variation of exchange parameters between the polyoxometalate and a simple dimer is much less pronounced.

Electrochemical properties: Attempts were made to elucidate the redox properties of the two complexes both in solution and in the solid state. The limited solubility of both complexes, placed restrictions upon the solution phase investigations. Our interest was to see if redox activity for the Fe^{III} centres and W-O framework for the POM complexes could be observed. The cyclic voltammogram obtained for **1** in a 0.1 M NH_4PF_6 DMSO solution (Figure 8a and 8b) showed a series of redox processes associated with the $Fe^{III/II}$ and bipyridine ligands of the $[Fe(bpy)_3]^{2+}$ moiety. The three monoelectronic bipyridine based redox processes were located at -1.515, -1.699 and -1.946 V (vs Ag/AgCl) with the $Fe^{III/II}$ at +0.780 V (vs Ag/AgCl), these are in close agreement with $[Fe(bpy)_3](PF_6)_2$ under the same experimental conditions, as seen in Figure SI3. A single redox process at an $E_{1/2}$ of approximately -0.771 V vs Ag/AgCl (Figure 8a), was also observed. On comparison to the Fe^{III} Keggin parent POM $[PW_{11}O_{39}Fe^{III}(H_2O)]^{4-}$ under the same solution conditions this redox couple can be attributed to the Fe^{III}

center substituted into the POM cage. It was not possible however to view the redox switching of the other Fe(III) site within the compound or the W-O framework in solution. As a result solid state electrochemical measurements were conducted on **1** for this purpose.

Solid state electrochemical measurements were conducted in a variety of aqueous electrolyte systems upon mechanically attached crystals of **1**. In a range of 1 M aqueous electrolyte systems, such as $LiClO_4$, the POM exhibited only a clear redox wave associated with the $Fe^{III/II}$ couple of the $[Fe(bpy)_3]^{2+}$ moiety. In order to view any redox activity for the $[PW_{11}O_{39}Fe_2^{III}(OH)bpy)_2]^{2-}$ POM, the attached microcrystals were cycled electrochemically in a range of aqueous buffer solutions from pH 2 to 4. In pH 4, the presence of what is believed to be a monoelectronic wave, at $E_{1/2}$ = -0.140 V, associated with the $Fe^{III/II}$ within the Keggin cage, is observed. In addition two bielectronic waves associated with the reduction of the tungsten-oxo framework with $E_{1/2}$ values of -0.590 and -0.834 V, are clearly seen in Figure 9a. The latter two waves were found to be pH dependent in nature, this is well know for the redox activity of the tungsten-oxo processes for the polyoxotungstates in solution.[38] Shifts of 65 to 75 mV per decade change in pH were observed for both of these waves thereby indicating the addition of two H^+ during each reduction step. This is similar to the unfunctionalised Fe^{III} Keggin POM. Scanning in a positive direction in this buffer solutions

revealed the monoelectronic wave associated with the $Fe^{III/II}$ of the cationic $[Fe(bpy)_3]^{2+}$ moiety, with a pH independent $E_{1/2}$ of +0.774 V (Figure 9b). The solid state behavior of this complex agrees well with the electrochemical properties of the $[Fe(bpy)_3]^{2+}$ and $[PW_{11}O_{39}Fe^{III}(H_2O)]^{4-}$ salts under the same conditions with little shift in redox potentials.

The inherent insolubility of **2** curtailed the solution phase electrochemistry of this complex to be investigated. As a result, the solid state electrochemical behaviour of **2** was investigated in buffered solutions so as to view the redox activity of this complex. In pH 2 buffer the attached microcrystals of **2** exhibited two bielectronic W-O processes with $E_{1/2}$ values of –0.410 and –0.645 V, and two redox couples at +0.044 V and +0.768 V, as seen in Figure 10. The latter being due to the redox switching of the Fe^{II} in the $[Fe^{II}(dmbpy)_3]^{2+}$ cation whilst the former is due to the Fe^{III} centres within the POM itself. The number of electrons involved in each process is difficult to ascertain due to the complexes inherent insolubility.

Conclusion.

The synthesis of $[PW_{11}O_{39}Fe_2^{III}(OH)(bpy)_2]^{2-}$, $[(PW_{11}O_{39})_2Fe_4^{III}O_2(dmbpy)_4]^{6-}$ and $[(PW_{11}O_{39})_2Fe_2^{III}O]^{10-}$ shows that hydrothermal conditions can be efficiently used for the synthesis of magnetic clusters encapsulated in POMs starting from vacant polyoxotungstate precursors. While to date the reaction of $[PW_{11}O_{39}]^{7-}$ towards first row transition metal ions M^{n+} under usual bench conditions has only led to

monosubstituted $\{PW_{11}O_{39}M(H_2O)\}$ anions, where M is disordered over the twelve metallic centers, hydrothermal conditions enhance the reactivity of the monolacunary precursor and allow the isolation of more sophisticated species. Using bipyridine-type ligands, an asymmetric dinuclear Fe(μ-O(W))(μ-OH)Fe complex where one iron atom is coordinated to a monovacant POM while the other is coordinated to two bipyridine ligands has been obtained, and a hybrid centrosymetric compound where a tetranuclear Fe_4 core is sandwiched between two POMs has also been isolated. The latter complex represents the first characterized butterfly like POM cluster. When non-coordinating tetramethylammonium cations replace bipyridine ligands in the synthetic process, the hydrothermal conditions have allowed to isolate a purely inorganic dinuclear Fe(μ-O)Fe cation where the magnetic core is sandwiched between two POMs. For the three compounds, the antiferromagnetic coupling constants between the paramagnetic centers have been determined and compared with related non-POM compounds. Particularly, this comparison, combined with DFT calculations has confirmed that metallic centers bridged by an oxo ligand coming from the POM are weakly coupled. This is due to long distances between the magnetic center and the oxygen atom of the POM but also to the important mixing of bridging oxygen orbitals with orbital of POM tungsten atoms. Electrochemical experiments on the hybrid complexes have allowed a partial determination of the redox waves associated with the metallic

centers and the bipyridine ligands constituting **1** and **2**. Our attention focuses now on other lacunary precursors as building units in order to increase the nuclearity of the magnetic clusters.

Experimental Section

Synthesis. $K_7[\alpha\text{-}PW_{11}O_{39}]\cdot 14H_2O$ was prepared according to a published procedure.[39] The hydrothermal syntheses were carried out in polytetrafluoroethylene lined stainless steel containers under autogeneous pressure. The 23 mL vessel was filled to approximatively 25 % volume capacity (V_i = 6 mL), All reactants were stirred briefly before heating. The samples were heated for 60 h at 160°C and cooled to room temperature over a period of 40 h. The pH mixture was measured before (pH_i) and after the reaction (pH_f). The products were isolated by filtration and washed with ethanol.

$[Fe^{II}(bpy)_3][PW_{11}O_{39}Fe_2^{III}(OH)(bpy)_2]\cdot 12H_2O$ (1) : a mixture of $K_7PW_{11}O_{39}\cdot 14H_2O$ (0.550 g, 0.175 mmol), $Fe_2(SO_4)_3$ (0.103 g, 0.257 mmol), 2,2′-bpy (0.135 g, 0.864 mmol) and H_2O was stirred and the pH was adjusted to 3 with 2M KOH (pH_f = 2). Dark red parallelepipedic crystals (0.360 g, yield 58% based on W) were collected by filtration. The crystals are purified by a gentle heating (50°C) in water in order to remove water soluble orange crystals which cocrystallize in small quantities with **1**. IR (KBr pellets): ν = 3116 (w), 3046 (w), 2921 (w), 2851 (w), 1471 (m), 1443 (s), 1383 (w), 1316 (w), 1265 (w), 1245

(w), 1174 (sh), 1157 (w), 1066 (m), 1027 (w), 993 (sh), 959 (m), 880 (m), 817 (s), 798 (sh), 761 (sh), 730 (w), 690 (w), 670 (sh), 650 (w), 591 (w), 549 (w), 512 (m) cm^{-1}; elemental analysis calcd (%) for $C_{50}H_{65}N_{10}Fe_3O_{52}PW_{11}$ (3858.85): C 15.56, H 1.69, N 3.63, Fe 4.34, P 0.80, W 52.40; found: C 15.92, H 1.27, N 3.73, Fe 4.63, P 0.87, W 52.20.

$(Hdmbpy)_2[Fe^{II}(dmbpy)_3]_2[(PW_{11}O_{39})_2Fe_4^{III}O_2(dmbpy)_4]\cdot 14H_2O$ (2): A mixture of $K_7PW_{11}O_{39}\cdot 14\ H_2O$ (0.550 g, 0.175 mmol), $Fe_2(SO_4)_3$ (0.103 g, 0.257 mmol), 5,5′-dimethyl-2,2′-bpy (0.140 g, 0.760 mmol) and H_2O was stirred and the pH was adjusted to 3 with 2M KOH (pH_f = 3). Dark red parallelepipedic crystals (0.360 g, yield 57% based on W) were collected by filtration. IR (KBr pellets): ν = 3120 (w), 3100 (w), 3080 (w), 3060 (w), 3045 (w), 2921 (w), 2855 (w), 1475 (m), 1447 (w), 1382 (w), 1311 (w), 1240 (m), 1235 (sh), 1149 (m),1084 (sh), 1064 (m), 958 (m), 885 (m), 808 (s), 729 (m), 701 (w), 666 (w), 652 (sh), 582 (m), 524 (m), 504(sh) cm^{-1}; elemental analysis calcd (%) for $C_{144}H_{174}N_{24}Fe_6O_{94}P_2W_{22}$ (8186.56): C 21.13, H 2.14, N 4.10, Fe 4.09, P 0.76, W 49.40; found: C 20.56, H 1.88, N 3.84, Fe 3.95, P 0.73, W 47.92.

$H_2[Fe^{II}(dmbpy)_3]_2[(PW_{11}O_{39})_2Fe_4^{III}O_2(dmbpy)_4]\cdot 10H_2O$ (3): A mixture of $K_7PW_{11}O_{39}\cdot 14\ H_2O$ (0.550 g, 0.175 mmol), $Fe_2(SO_4)_3$ (0.103 g, 0.257 mmol), 5,5′-dimethyl-2,2′-bpy (0.080 g, 0.434 mmol) and H_2O was stirred and the pH was adjusted to 3 with 2M KOH (pH_f = 3). Dark red parallelepipedic crystals (0.150 g, yield 22% based

on W) were collected by filtration. IR (KBr pellets): ν = 3120 (w), 3100 (w), 3080 (w), 3060 (w), 3045 (w), 2921 (w), 2855 (w), 1475 (m), 1447 (w), 1382 (w), 1311 (w), 1240 (m), 1235 (sh), 1149 (m),1084 (sh), 1064 (m), 958 (m), 885 (m), 808 (s), 729 (m), 701 (w), 666 (w), 652 (sh), 582 (m), 524 (m), 504(sh) cm^{-1}; elemental analysis calcd (%) for $C_{120}H_{142}N_{20}Fe_6O_{90}P_2W_{22}$ (7746.03) C 18.61, H 1.85,N 3.62, Fe 4.33, P 0.80, W 52.21; found: C 19.55, H 1.75, N 3.78, Fe 4.38, P 0.81, W 50.85.

$[N(CH_3)_4]_{10}[(PW_{11}O_{39})_2Fe_2^{III}O]\cdot 12H_2O$ (4): A mixture of $K_7PW_{11}O_{39}\cdot 14\ H_2O$ (0.550 g, 0.175 mmol), $Fe_2(SO_4)_3$ (0.103 g, 0.257 mmol), tetramethylammonium bromide (0.135 g, 0.878 mmol) and H_2O was stirred and the pH was adjusted to 4 with 2M KOH (pH_f = 2.5). Parallelepipedic yellow crystals (0.310 g, yield 56 % based on W) were collected by filtration. IR (KBr pellets, ν/ cm^{-1}): 3034 (m), 2958 (w), 2922 (w), 2854 (w), 2768(w), 2763 (w), 2655 (w), 2589 (w), 2519 (w), 2487 (w), 1629 (w), 1486 (s), 1450 (m), 1418 (m), 1384 (m), 1286 (m), 1262 (m), 1093 (sh), 1057 (m), 956 (s), 815 (s), 759 (w), 729 (sh), 690 (w), 668 (sh), 595 (m), 521 (w), 489 (sh), 456 (m), 412 (m); elemental analysis calcd (%) for $C_{40}H_{144}N_{10}Fe_2O_{91}P_2W_{22}$ (6439.73) C 7.46, H 2.25,N 2.17, Fe 1.73, P 0.96, W 62.80; found: C 7.47, H 2.11, N 2.15, Fe, P, W.

X-ray crystallography. Intensity data collection was carried out with a Bruker Nonius X8 APEX 2 diffractometer for **1-4,** equipped with a CCD bidimensional detector using the

monochromatized wavelength λ(Mo Kα) = 0.71073 Å. All the data were recorded at room temperature. The absorption correction was based on multiple and symmetry-equivalent reflections in the data set using the SADABS program[40] based on the method of Blessing.[41] The structures were solved by direct methods and refined by full-matrix least-squares using the SHELX-TL package.[42] In all the structures there is a discrepancy between the formulae determined by elemental analysis and the formulae deduced from the crystallographic atom list because of the difficulty in locating all the disordered water molecules. These molecules have been refined with partial occupancy factors. In the structure of **2**, it has been possible to locate the free $Hdmby^+$ ions, the attribution of the two N positions among the four possible ones has been made according to the considerations of distances. The structure of **3** has been solved in the noncentrosymmetric *P*1 space group although an analysis by Platon suggests *P*–1 because in the centrosymmetric space group the bpy ligands were too close in space. Crystallographic data are given in Table 3. Selected bond distances are listed in Table 1 and 2. CCDC-649965 – 649968 contain the supplementary crystallographic data for the structures of **1**-**4**, respectively, described in this paper. These data can be obtained free of charge from the Cambridge Crystallographic Data Centre via www.ccdc.cam.ac.uk/data_request/cif.

TGA measurements: Thermogravimetry was carried out under N_2/O_2 (1:1) flow (60 mL min^{-1}) with a Perkin-Elmer electrobalance TGA-7 at a heating rate 10 °C min^{-1} up to 800°C.

Magnetic measurements: Magnetic susceptibility measurements were carried out with a Quantum Design SQUID Magnetometer with an applied field of 1000 Oe using powder samples pressed in pellets to avoid preferential orientation of the crystallites. The independence of the susceptibility value with regard to the applied field was checked at room temperature. The susceptibility data were corrected from the diamagnetic contributions as deduced by using Pascal's constant tables. 4.85%, 4.07% and 0.04% of paramagnetic Fe^{III} impurities were taken into account for the fit of **1**, **2** and **4**, respectively.

Computational details: Electronic structure calculations were performed with GAUSSIAN 03 package.[43] The Fe and W atoms were described with LANL2DZ basis set with LANL2 effective core potentials, whereas 6-31g basis set was used for all other atoms. The three-parameter exchange-correlation functional of Becke based on the correlation functional of Lee, Yang, and Parr (B3LYP),[44] which is known to be suited for the estimation of exchange interactions, was used in all calculations. The exchange parameters were evaluated following the DFT-broken symmetry method.[45]

Electrochemical measurements: The reference electrode that was employed in organic solvents was a silver wire in contact with a solution of $AgNO_3$ (0.01 M) and 0.1 M of the same supporting

electrolyte as employed in the cell. For aqueous electrochemistry a silver/silver chloride (3M KCl) reference electrode was used. A carbon (d = 3 mm) working electrode was employed which was polished, prior to use, with 0.05 μm alumina and rinsed with deionised water. The auxiliary electrode material was a platinum wire. A CH 660A potentiostat was employed for all electrochemical experiments. All solutions were degassed with pure argon for 15 min prior to electrochemical experiments. For solid state voltammetric measurements, a slurry of the complexes was first prepared and then transferred onto the electrode surface. Before electrochemical studies the coatings were allowed to dry. After use, the electrode surface was renewed by rinsing with acetone, polishing with 0.05 μm alumina and then sonicated in deionised water.

References

[1] M. T. Pope, *Heteropoly and Isopoly Oxometalates*, Springer, Berlin, 1983.

[2] D.-L. Long, E. Burkholder, L. Cronin, *Chem. Soc. Rev.* **2007**, *36*, 105.

[3] B. Godin, Y.-G. Chen, J. Vaissermann, L. Ruhlmann, M. Verdaguer, P. Gouzerh, *Angew. Chem. Int. Ed.* **2005**, *44*, 3072.

[4] a) A. Muller, F. Peters, M. T. Pope, D. Gatteschi, *Chem. Rev.* **1998**, 240; b) J. M. Clemente-Juan, E. Coronado, *Coord. Chem. Rev.* **1999**, *193-195*, 361.

[5] See for example the recent special issue on POMs of *J. Mol. Catal. A*: *Chem.* **2007**, *262*, 1-242.

[6] P. Mialane, A. Dolbecq, F. Sécheresse, *Chem. Commun.* **2006**, *33*, 3477.

[7] a) P.-Q. Zheng, Y.-P. Ren, L.-S. Long, R.-B. Huang, L.-S. Zheng, *Inorg. Chem.* **2005**, *44*, 1190; b) H. Jin, C. Qin, Y.-G. Li, E.-B. Wang, *Inorg. Chem. Commun.* **2006**, *9*, 482; c) X.-J. Kong, Y.-P. Ren, P.-Q. Zheng, Y.-X. Long, L.-S. Long, R.-B. Huang, L.-S. Zheng, *Inorg. Chem.* **2006**, *45*, 10702.

[8] C. Ritchie, E. Burkholder, P. Kögerler, L. Cronin, *Dalton Trans.* **2006**, 1712.

[9] S.-T. Zheng, D.-Q. Yuan, H.-P. Jia, J. Zhang, G.-Y. Yang, *Chem. Commun.* **2007**, 1858.

[10] a) R. N. Devi, E. Burkholder, J. Zubieta, *Inorg. Chim. Acta* **2003**, *348*, 150; b) L. Lisnard, A. Dolbecq, P. Mialane, J. Marrot, F. Sécheresse, *Inorg. Chim. Acta*. **2004**, *357*, 845.

[11] a) Y. Xu, J.-Q. Xu, K.-L. Zhang, Y. Zhang, X.-Z. You, *Chem. Commun*. **2000**, 153; b) B. Yan, Y. Xu, X. Bu, N. K. Goh, L. S. Chia, G. D. Stucky, *Dalton Trans*. **2001**, 2003; c) E. Burkholder, V. Golub, C. J. O'Connor, J. Zubieta, *Inorg. Chem. Commun*. **2004**, *7*, 363; d) L. Lisnard, A. Dolbecq, P. Mialane, J. Marrot, E. Codjovi, F. Sécheresse *Dalton Trans.* **2005**, 3913.

[12] J.-P. Wang, Q. Ren, J.-W. Zhao, J.-Y. Niu, *Inorg. Chem. Commun*. **2006**, *9*, 1281.

[13] L. S. Felices, P. Vitoria, J. M. Gutiérrez-Zorrilla, L. Lezama, S. Reinoso, *Inorg. Chem*. **2006**, *45*, 7748.

[14] S. Chang, C. Qin, E. Wang, Y. Li, X. Wang, *Inorg. Chem. Commun*. **2006**, *9*, 727.

[15] a) L.-H. Bi, U. Kortz, S. Nellutla, A. C. Stowe, J. v. Tol, N. S. Dala, B. Keita, L. Nadjo, *Inorg. Chem.* **2005**, *44*, 896; b) M. Prinz, A. F. Takács, J. Schnack, I. Balasz, E. Burzo, U. Kortz, K. Kuepper, M. Neumann, *J. Appl. Phys*. **2006**, *99*, 08J505.

[16] a) U. Kortz, M. G. Savelieff, B. S. Bassil, B. Keita, L. Nadjo, *Inorg. Chem.* **2002**, *41*, 783; b) B. Keita, I. M.

Mbomekalle, L. Nadjo, T. M. Anderson, C. Hill, *Inorg. Chem*. **2004**, *43*, 3257.

[17] a) T. M. Anderson, X. Zhang, K. I. Hardcastle, C. Hill *Inorg. Chem*. **2002**, *41*, 2477; b) N. M. Okun, T. M. Anderson, C. Hill, *J. Am. Chem. Soc*. **2003**, *125*, 3194; c) B. Botar, Y. V. Geletii, P. Kögerler, D. G. Musaev, K. Morokuma, I. A. Weinstock, C. Hill, *J. Am. Chem. Soc*. **2006**, *128*, 11268; d) M. Bonchio, M. Carraro, A. Sartorel, G. Scorrano, U. Kortz, *J. Mol. Catal. A*: *Chem*. **2007**, *262*, 36; e) I. C. M. S. Santos, J. A. F. Gamelas, M. S. S. Balula, M. M. Q. Simões, M. G. P. M.S. Neves, J. A. S. Cavaleiro, A. M. V. Cavaleiro, *J. Mol. Catal. A*: *Chem*. **2007**, *262*, 41.

[18] a) N. Mizuno, K. Yamaguchi, K. Kamata, *Coord. Chem. Rev*. **2005**, 249; b) M. Bonchio, M. Carraro, A. Sartorel, G. Scorrano, U. Kortz, *J. Mol. Catal. A*: *Chem*. **2006**, *251*, 93.

[19] a = 13.3642(2), b = 17.2873(3), c = 20.3975(4) Å, a = 90, β = 77.604(1), γ = 90°, V = 4602.6 $Å^3$.

[20] (a) F. Zonnevijlle, C. M. Tourné, G. F. Tourné, *Inorg. Chem*., 1982, **21**, 2742, (b) J. A. Gamelás, F. A. A. Couto, M. N. Trovão, A. M. V. Cavaleiro, J. A. S. Cavaleiro, J. D. Pedrosa de Jesus, *Thermochimica Acta*, **1999**, *326*, 165.

[21] F. Zonnevijlle, C. M. Tourné, G. F. Tourné, *Inorg. Chem*. **1982**, *21*, 2751.

[22] a) Z.-E. Lin, J. Zhang, Y.-Q. Sun and G.-Y. Yang, *Inorg. Chem.*, 2004, *43*, 797; b) W. Yang and C. Lu, *Inorg. Chem.*, **2002**, *41*, 5638; c) L. Lisnard, A. Dolbecq, P. Mialane, J. Marrot, E. Rivière, S. A. Borshch, S. Petit, V. Robert, C. Duboc, T. McCormac, F. Sécheresse, *Dalton Trans*. **2006**, 5141.

[23] B. N. Figgis, B. W. Skelton, A. H. White, *Aust. J. Chem.* **1978**, *31*, 57.

[24] N. E. Brese, M. O'Keeffe, *Acta Crystallogr.* **1991**, *B47*, 192.

[25] a) J. K. McCusker, J. B. Vincent, E. A. Schmitt, M. L. Mino, K. Shin, D. K. Coggin, P. M. Hagen, J. C. Huffman, G. Christou, D. N. Hendrickson, *J. Am. Chem. Soc*. **1991**, *113*, 3012; b) A. K. Boudalis, N. Lalioti, G. A. Spoyroulias, C. P. Raptopoulou, A. Terzis, A. Bousseksou, V. Tangoulis, J.-P. Tuchagues, S. P. Perlepes, *Inorg. Chem.* **2002**, *41*, 6474; c) J. Overgaard, D. E. Hibbs, E. Rentschler, G. A. Timco, F. K. Larsen, *Inorg. Chem*. **2003**, *42*, 7593; d) T. C. Stamatatos, A. K. Boudalis, Y. Sanakis, C. P. Raptopoulou, *Inorg. Chem*. **2006**, *45*, 7372.

[26] F. Zonnevijlle, C. M. Tourné, G. F. Tourné, *Inorg. Chem*. **1982**, *21*, 2751.

[27] O. A. Kholdeeva, G. M. Maksimov, R. I. Maksimovskaya, L. A. Kovalena, M. A. Fedotov, V. A. Grigoriev, C. L. Hill, *Inorg. Chem.* **2000**, *39*, 3828.

[28] O. A. Kholdeeva, G. M. Maksimov, R. I. Maksimovskaya, P. Vanina, T. A. Trubitsina, D. Yu Naumov, B. A. Kolesov, N. S. Antonova, J.J. Carbó, J. M. Poblet, *Inorg. Chem.* **2006**, *45*, 7224.

[29] a) M. Sadakane, M. Higashijima, *Dalton Trans.* **2003**, 659 ; b) M. Sadakane, D. Tsukuma, M. H. Dickman, B. S. Bassil, U. Kortz, M. Capron, W. Ueda, *Dalton Trans.* **2007**, advance article.

[30] R = $[\Sigma(\chi_M T_{calc} - \chi_M T_{obs})^2 / \Sigma(\chi_M T_{obs})^2]$

[31] a) D. M. Kurtz, *Chem. Rev.* **1990**, *90*, 585; b) E. I. Solomon, T. C. Brunold, M. I. Davis, J. N. Kemsley, S. K. Lee, N. Lehnert, F. Neese, A. J. Skulan, Y.-S. Yang, J. Zhou, *Chem. Rev.* **2000**, *100*, 235; c) E. Y. Tshuva, S. J. Lippard, *Chem. Rev.* **2004**, *104*, 987.

[32] A. Stubna, D.-H. Jo, M. Costas, W. W. Brenessel, H. Andres, E. L. Bominaar, E. Münck, L. Que, Jr. *Inorg. Chem.* **2004**, *43*, 3067.

[33] (a) S. M. Gorun, S. J. Lippard, *Inorg. Chem.* **1991**, *30*,1625. (b) H. Weihe, H. U. Güdel *J. Am. Chem. Soc.* **1997**, *119*, 6539. (c) R. Werner, S. Ostrovsky, K. Griesar W. Haase, *Inorg. Chim. Acta*, **2001**, *326*, 78.

[34] J. Jullien, G. Juhász, P. Mialane, E. Dumas, C. R. Mayer, J. Marrot, E. Rivière, E. L. Bominaar, E. Münck, F. Sécheresse, *Inorg. Chem.* **2006**, *45*, 6922.

[35] T. Cauchy, E. Ruiz, S. Alvarez, *J. Am. Chem. Soc*. **2006**, *128*, 15722.

[36] A. Hazell, K. B. Jensen, C. J. McKenzie, H. Toftlund, *Inorg. Chem.*, **1994**, *33*, 3127.

[37] E. M. Zueva, H. Chermette, S. A. Borshch, *Inorg. Chem.* **2004**, *43*, 2834.

[38] N. Fay, E. Dempsey, T. McCormac, *J. Electroanal. Chem.* **2005**, *574*, 359.

[39] R. Contant, *Can. J. Chem*. **1987**, *65*, 570.

[40] G. M. Sheldrick, SADABS ; program for scaling and correction of area detector data, University of Göttingen, Germany, 1997.

[41] R. Blessing, *Acta Crystallogr.*, **1995**, *A51*, 33.

[42] G. M. Sheldrick, SHELX-TL version 5.03, Software Package for the Crystal Structure Determination, Siemens Analytical X-ray Instrument Division : Madison, WI USA, 1994.

[43] M. J. Frisch, G. W. Trucks, H. B. Schlegel, G. E. Scuseria, M. A. Robb, J. R. Cheeseman, J. A. Montgomery, Jr., T. Vreven, K. N. Kudin, J. C. Burant, J. M. Millam, S. S. Iyengar, J. Tomasi, V. Barone, B. Mennucci, M. Cossi, G. Scalmani, N. Rega, G. A. Petersson, H.

Nakatsuji, M. Hada, M. Ehara, K. Toyota, R. Fukuda, J. Hasegawa, M. Ishida, T. Nakajima, Y. Honda, O. Kitao, H. Nakai, M. Klene, X. Li, J. E. Knox, H. P. Hratchian, J. B. Cross, V. Bakken, C. Adamo, J. Jaramillo, R. Gomperts, R. E. Stratmann, O. Yazyev, A. J. Austin, R. Cammi, C. Pomelli, J. W. Ochterski, P. Y. Ayala, K. Morokuma, G. A. Voth, P. Salvador, J. J. Dannenberg, V. G. Zakrzewski, S. Dapprich, A. D. Daniels, M. C. Strain, O. Farkas, D. K. Malick, A. D. Rabuck, K. Raghavachari, J. B. Foresman, J. V. Ortiz, Q. Cui, A. G. Baboul, S. Clifford, J. Cioslowski, B. B. Stefanov, G. Liu, A. Liashenko, P. Piskorz, I. Komaromi, R. L. Martin, D. J. Fox, T. Keith, M. A. Al-Laham, C. Y. Peng, A. Nanayakkara, M. Challacombe, P. M. W. Gill, B. Johnson, W. Chen, M. W. Wong, C. Gonzalez, and J. A. Pople, Gaussian, Inc., Wallingford CT, 2004.

[44] a) C. T. Lee, W. T. Yang and R. G. Parr, *Phys. Rev. B*, **1988**, *37*, 785; b) A. D. Becke, *J. Chem. Phys.*, **1993**, *98*, 5648.

[45] (a) L. Noodleman, J. G. Norman Jr. *J. Chem. Phys*. **1979**, *70*, 4903. (b) L. Noodleman, *J. Chem. Phys*. **1981**, *74*, 5737.

Figure Captions.

Figure 1 Mixed ball and stick and polyhedral representation of the $[PW_{11}O_{39}Fe_2^{III}(OH)(bpy)_2]^{2-}$ anion in **1**; white octahedra WO_6, dark grey tetrahedron PO_4, medium grey spheres Fe, white spheres O, light grey spheres N, black spheres C.

Figure 2 a) Mixed ball and stick and polyhedral representation of the $[(PW_{11}O_{39})_2Fe_4^{III}O_2(dmbpy)_4]^{6-}$ anion common in **2** and **3**; white octahedra WO_6, dark grey tetrahedra PO_4, medium grey spheres Fe, white spheres O, light grey spheres N, black spheres C; b) view of the tetrameric butterfly complex sandwiched between the two monolacunary anions with atom labelling scheme; the carbon atoms of the organic ligand have been omitted for clarity; c) schematic representation of the Fe_4 core showing the two main exchange interactions, the star indicates symmetry related atoms.

Figure 3 Mixed ball and stick and polyhedral representation of the $[(PW_{11}O_{39})_2Fe_2^{III}O]^{10-}$ anion in **4**; white octahedra WO_6, dark grey tetrahedra PO_4, medium grey spheres Fe, white spheres O.

Figure 4 Plot of $\chi_M T$ versus T for compound **1** between 300 and 2 K. The solid line was generated from the best fit parameters given in the text.

Figure 5 Plot of $\chi_M T$ versus T for compound **2** between 300 and 2 K. The solid line was generated from the best fit parameters given in the text.

Figure 6 Error contour plots for different J_{wb} and J_{bb} values for the simulation of the magnetic susceptibility measurement of **3**.

Figure 7 Plot of $\chi_M T$ versus T for compound **4** between 300 and 2 K. The solid line was generated from the best fit parameters given in the text.

Figure 8 Cyclic voltammograms of a 2 mM solution of **1** in 0.1 M NH_4PF_6 at a bare carbon electrode (A = 0.0707 cm^2). Scan rate = 100 mV s^{-1}.

Figure 9 Solid state cyclic voltammograms of crystals of **1** adhered to a carbon electrode (A = 0.0707 cm^2) in buffer pH 4 solution. Scan rate = 100 mV s^{-1}.

Figure 10 Solid state cyclic voltammograms of crystals of **2** adhered to a carbon electrode (A = 0.0707 cm^2) in buffer pH 2 solution. Scan rate = 100 mV s^{-1}.

Table 1. Selected bond distances [Å] and angles (°) in 1, 2 and 4 associated to the representations of Figures 1-3.

1			
Fe(1)-O(14)	1.905(11)	Fe(2)-O(7)	1.915(11)
Fe(1)-O(37)	1.925(11)	Fe(2)-O(9)	1.941(12)
Fe(1)-O(9)	1.932(12)	Fe(2)-N(2)	2.104(13)
Fe(1)-O(10)	1.992(11)	Fe(2)-N(3)	2.109(14)
Fe(1)-O(7)	2.106(11)	Fe(2)-N(4)	2.151(16)
Fe(1)-O(25)	2.271(11)	Fe(2)-N(1)	2.157(14)
Fe(1)-Fe(2)	3.013(3)		
Fe(2)-O(7)-Fe(1)	97.05(5)	Fe(1)-O(9)-Fe(2)	102.1(5)
2			
Fe(1)-O(40)	1.926(9)	Fe(2)-O(40)	1.929(7)
Fe(1)-O(36)	1.944(11)	Fe(2)-O(40)	1.943(11)
Fe(1)-O(39)	1.955(9)	Fe(2)-N(12)	2.152(8)
Fe(1)-O(27)	2.007(10)	Fe(2)-N(15)	2.158(6)
Fe(1)-O(23)	2.030(10)	Fe(2)-N(1)	2.186(13)
Fe(1)-O(25)	2.472(10)	Fe(2)-N(26)	2.215(8)
Fe(1)-Fe(2)	3.491(5)	Fe(2)-Fe(2)	2.910(4)
Fe(2)-O(40)-Fe(1)	133.6(6)	Fe(2)-O(40)-Fe(2)*	97.4(4)
Fe(1)-O(40)-Fe(2)	129.0(4)		
4			
Fe(1)-O(79)	1.775(7)	Fe(2)-O(79)	1.767(7)
Fe(1)-O(39)	1.988(8)	Fe(2)-O(47)	1.969(8)
Fe(1)-O(17)	1.999(9)	Fe(2)-O(70)	1.976(9)
Fe(1)-O(9)	2.001(8)	Fe(2)-O(53)	2.002(9)
Fe(1)-O(30)	2.029(9)	Fe(2)-O(78)	2.010(8)
Fe(1)-O(11)	2.616(8)	Fe(2)-O(57)	2.594(9)
Fe(1)-Fe(2)	3.513(3)	Fe(2)-O(79)-Fe(1)	165.4(6)

Table 2. X-ray Crystallographic Data for 1-4.

	1	**2**	**3**	**4**
Formula	$C_{50}H_{45}Fe_3N_{10}O_{52}PW_1$ [1]	$C_{144}H_{146}Fe_6N_{24}O_{81}P_2W_{22}$	$C_{120}H_{120}Fe_6N_{20}O_{81}P_2W_{22}$	$C_{40}H_{144}Fe_2N_{10}O_{91}P_2W_2$ [2]
Fw [g]	3838.83	7950.59	7580.10	6439.73
Crystal system	Monoclinic	Monoclinic	Triclinic	Triclinic
Space group	*C*2/c	*C2/c*	*P*1	*P*-1
Z	8	4	1	2
T [K]	293	293	293	293
a [Å]	23.1859(8)	28.851(2)	13.3562(6)	13.1534(3)
b [Å]	13.9166(8)	36.971(3)	14.1707(6)	20.3426(6)
c [Å]	47.537(2)	20.947(2)	24.778(1)	24.0622(7)
α [°]	90	90	81.004(2)	94.2950(10)
β [°]	103.247(4)	118.229(4)	83.810(2)	97.1150(10)
γ [°]	90	90	65.434(2)	92.1570(10)
V [Å^3]	14931(1)	19686(3)	4207.9(3)	6363.7(3)
ρ_{calc} [g cm^{-3}]	3.416	2.683	2.991	3.361
μ [mm^{-1}]	17.573	13.325	15.576	20.136
Reflections collected	71279	75101	76836	160858
Unique reflections (R_{int})	22050(0.0720)	17344(0.1581)	37765(0.0508)	37375(0.0472)
Refined parameters	1029	1072	2178	1342
$R(F_o)$[a]	0.0701	0.0653	0.0610	0.0657
$R_w(F_o^2)$[b]	0.1758	0.1587	0.1576	0.1153

[a] $R_1 = \frac{\sum||F_o|-|F_c||}{\sum|F_c|}$; [b] $wR_2 = \sqrt{\frac{\sum w(F_o^2 - F_c^2)^2}{\sum w(F_o^2)^2}}$ with $\frac{1}{w} = \sigma^2 F_o^2 + aP^2 + bP$ and $P = \frac{F_o^2 + 2F_c^2}{3}$ a = 0.0991, b = 601.63 for **1**, a = 0.1195, b = 0 for **2**, a = 0.1160, b = 0 for **3**, a = 0.0795, b = 272.69 for **4.**

Graphical Abstract

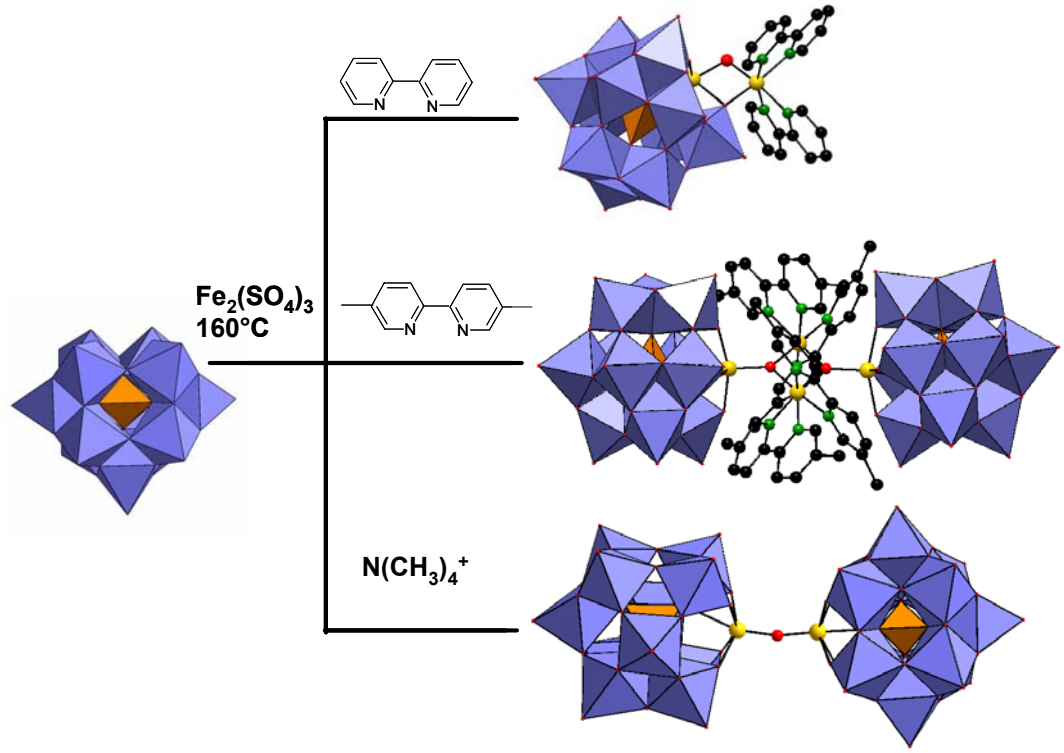

Ligand and/or counter-ion? The nature of the bridging units between Fe^{III} ions encapsulated within monolacunary phosphotungstates depends on whether chelating amines or non coordinating tetramethylammonium cations are introduced in the reaction medium.

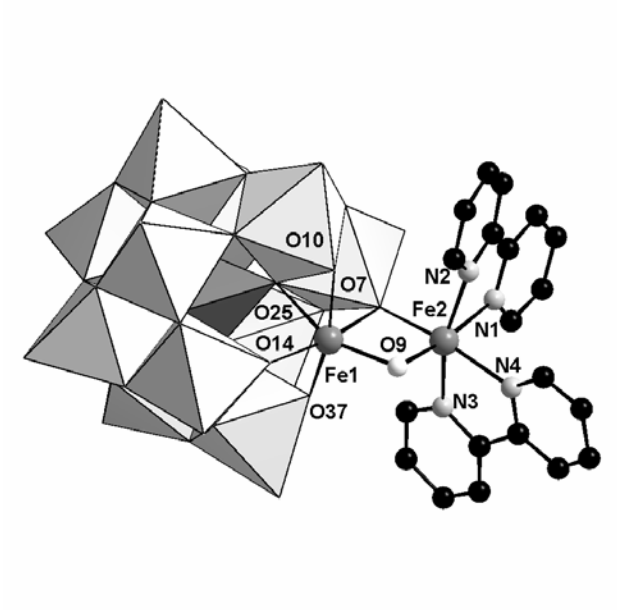

Figure 1

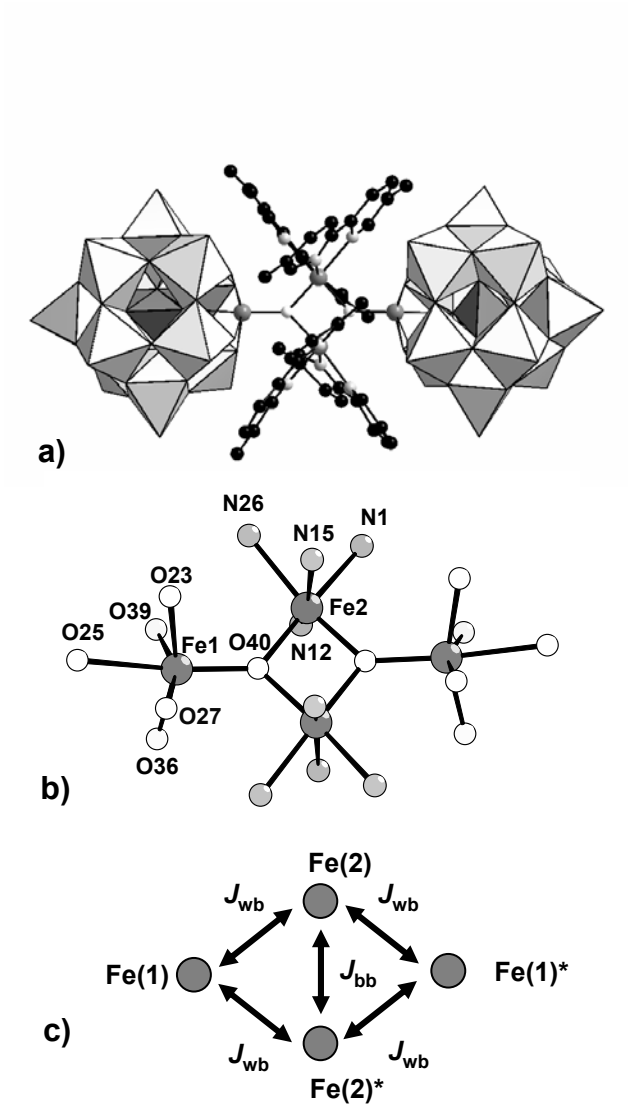
a)
N26
N15
N1
O23
O39
O25
Fe1
O40
Fe2
N12
O27
O36
b)
Fe(2)
J_{wb}
J_{wb}
Fe(1)
J_{bb}
Fe(1)*
J_{wb}
J_{wb}
Fe(2)*
c)

Figure 2

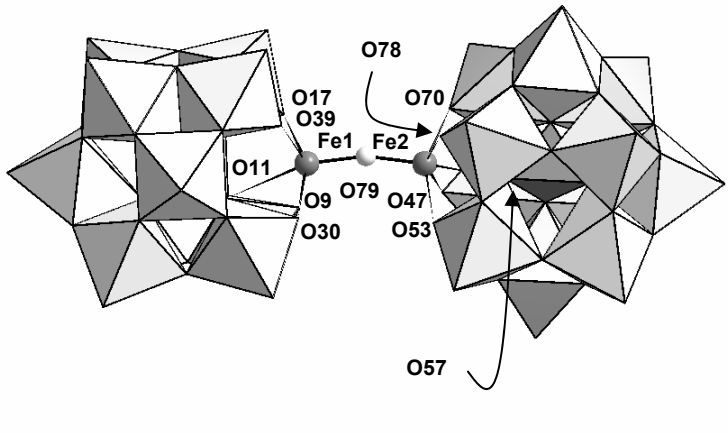

Figure 3

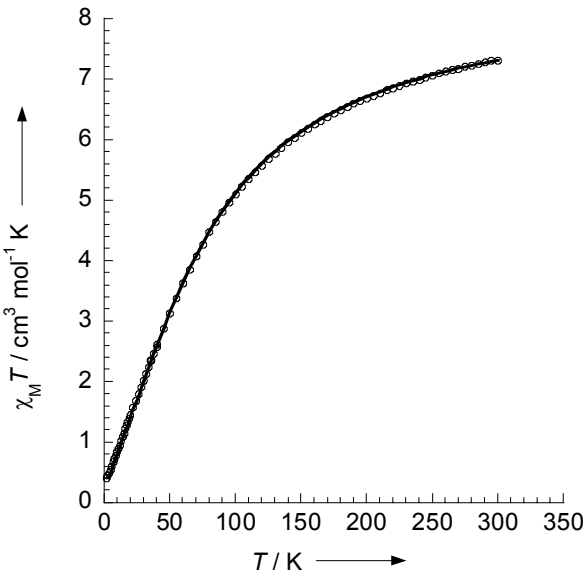

Figure 4

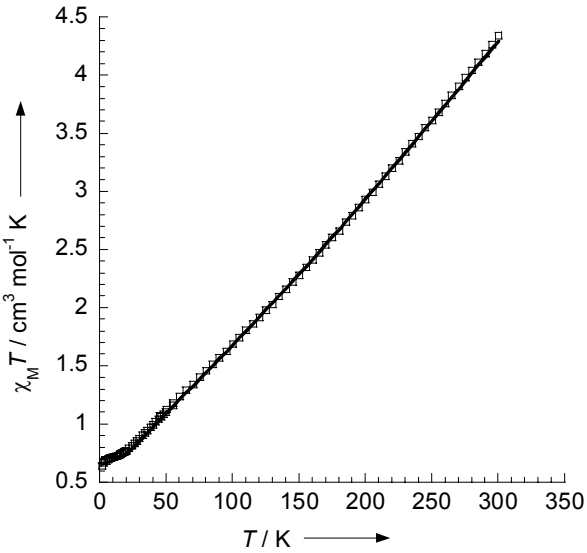
4.5
4
3.5
3
2.5
2
1.5
1
0.5
0
50
100
150
200
250
300
350
$\chi_M T$ / cm^3 mol^{-1} K
T / K

Figure 5

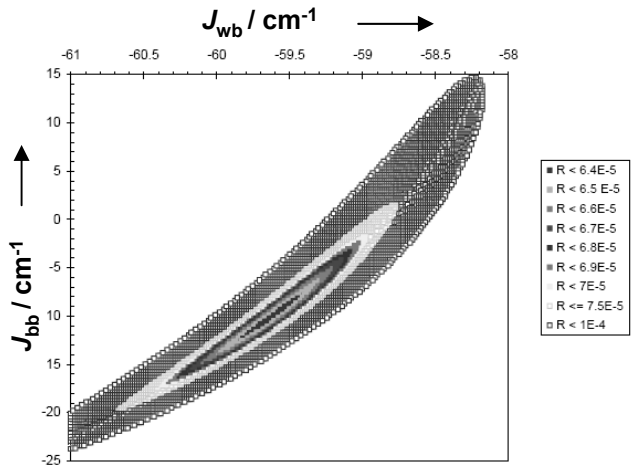
J_{wb} / cm^{-1}
-61
-60.5
-60
-59.5
-59
-58.5
-58
15
10
5
0
-5
10
15
-20
-25
J_{bb} / cm^{-1}
R < 6.4E-5
R < 6.5 E-5
R < 6.6E-5
R < 6.7E-5
R < 6.8E-5
R < 6.9E-5
R < 7E-5
R <= 7.5E-5
R < 1E-4

Figure 6

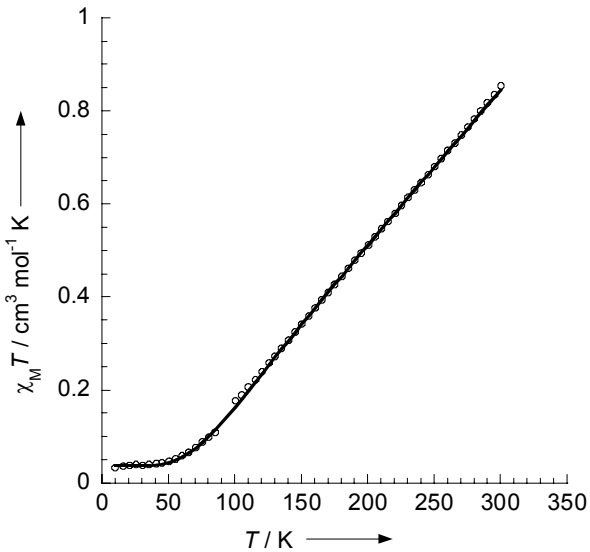

Figure 7

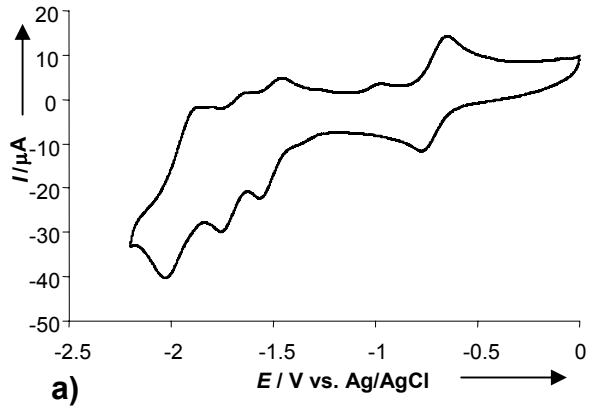
20
10
0
-10
-20
-30
-40
-50
I /µA
-2.5
-2
-1.5
-1
-0.5
0
E / V vs. Ag/AgCl
a)

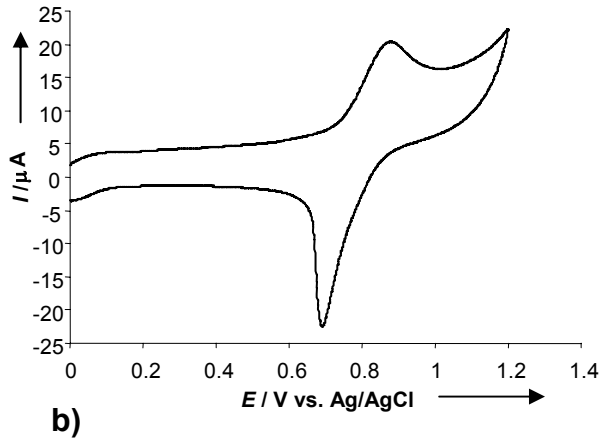
25
20
15
10
5
0
-5
-10
-15
-20
-25
I /µA
0
0.2
0.4
0.6
0.8
1
1.2
1.4
E / V vs. Ag/AgCl
b)

Figure 8

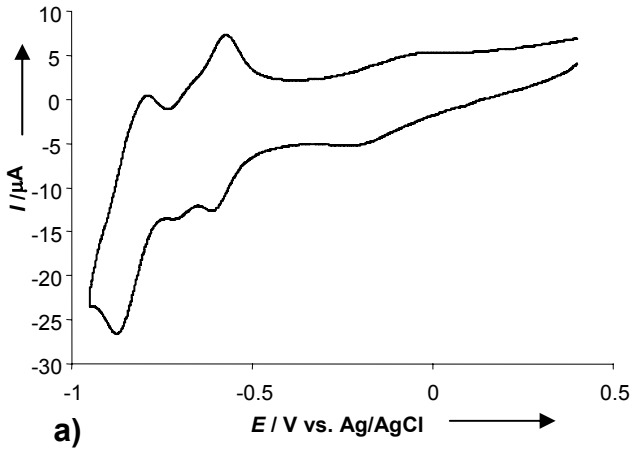
10
5
0
-5
-10
-15
-20
-25
-30
I /µA
-1
-0.5
0
0.5
E / V vs. Ag/AgCl
a)

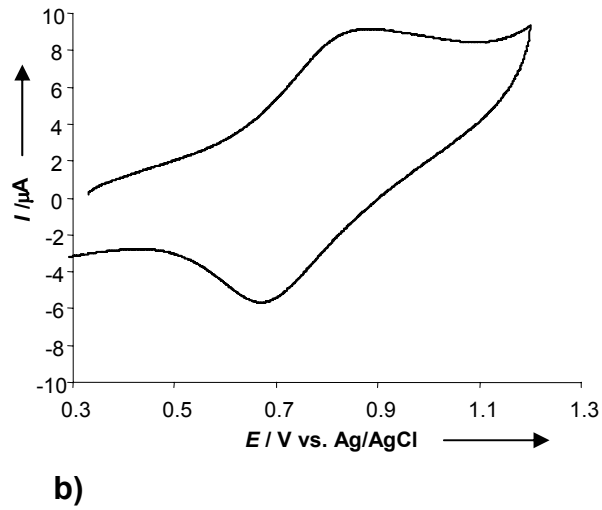
10
8
6
4
2
0
-2
-4
-6
-8
-10
I /µA
0.3
0.5
0.7
0.9
1.1
1.3
E / V vs. Ag/AgCl
b)

Figure 9

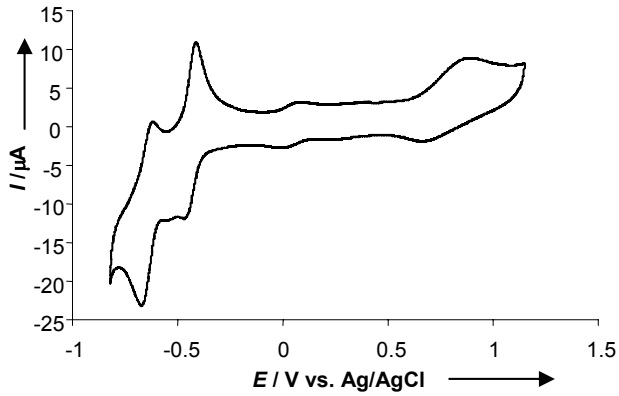

Figure 10

Supplementary Information.

Fe_2 and Fe_4 Clusters Encapsulated in Vacant Polyoxotungstates: Hydrothermal Synthesis, Magnetic, Electrochemical Properties, and DFT calculations

Céline Pichon,[a] Anne Dolbecq,*[a] Pierre Mialane,[a] Jérôme Marrot,[a] Eric Rivière,[b] Monika Goral,[c] Monika Zynek, [c] Timothy McCormac,[c] Serguei A. Borshch,[d] Ekaterina Zueva,[e] and Francis Sécheresse[a]

Figure SI1
Infrared spectra of 1 - 4

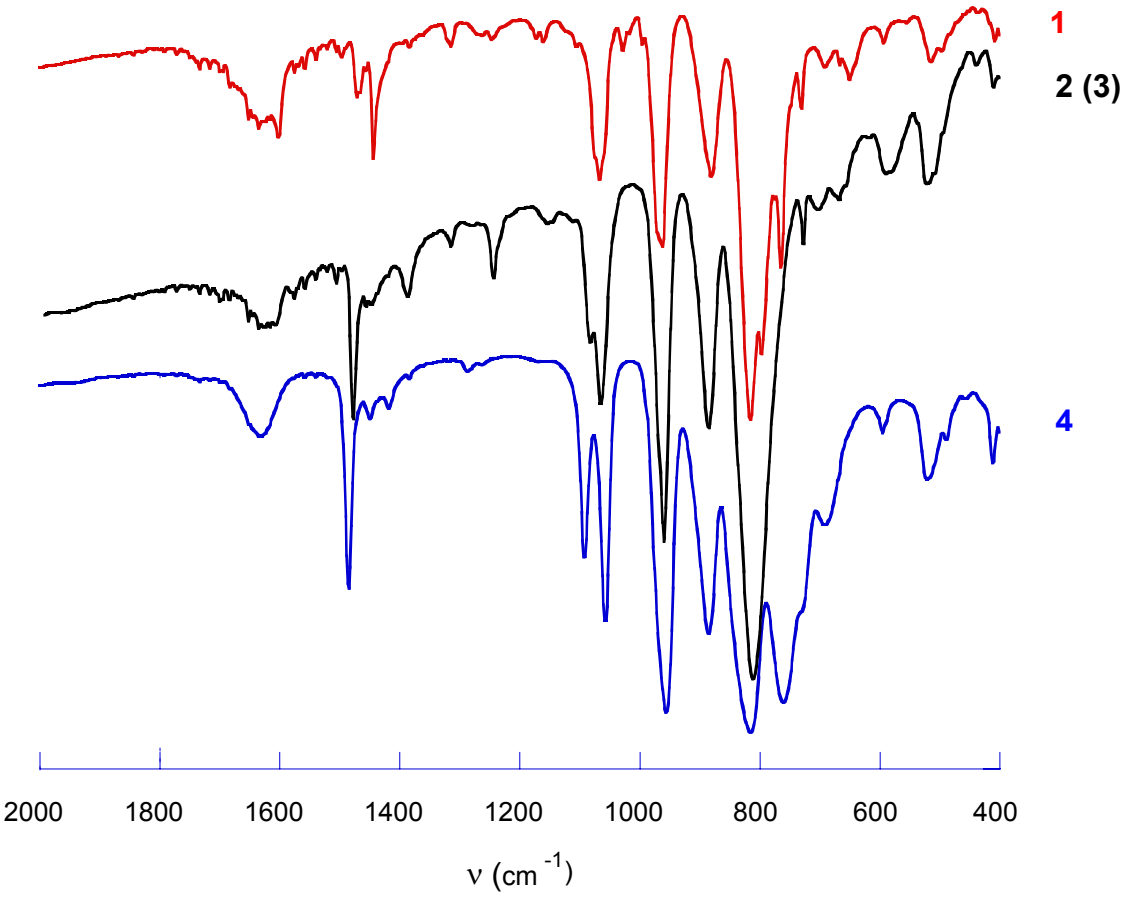

Figure SI2
Thermogravimetric analysis for 1-4

1 :

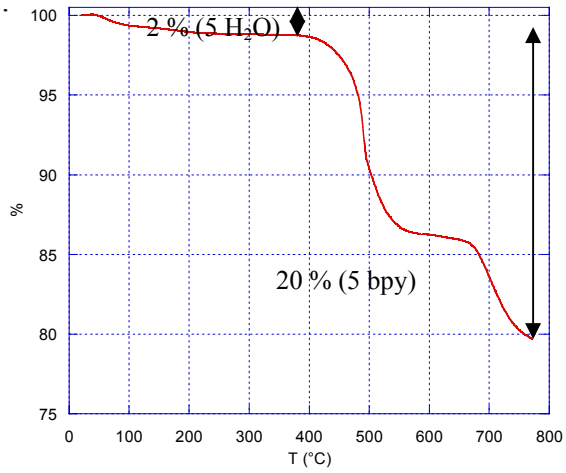

2 :

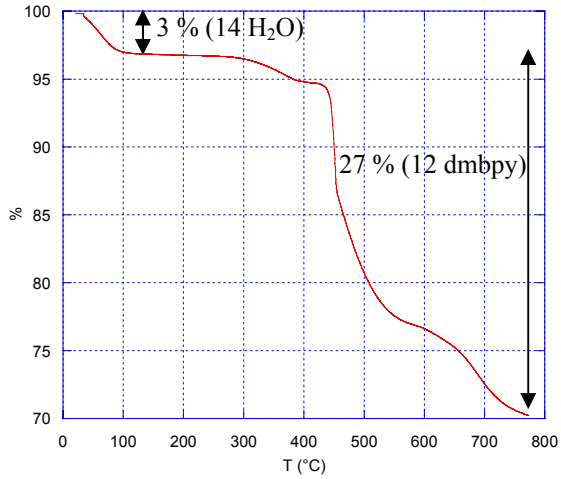

3 :

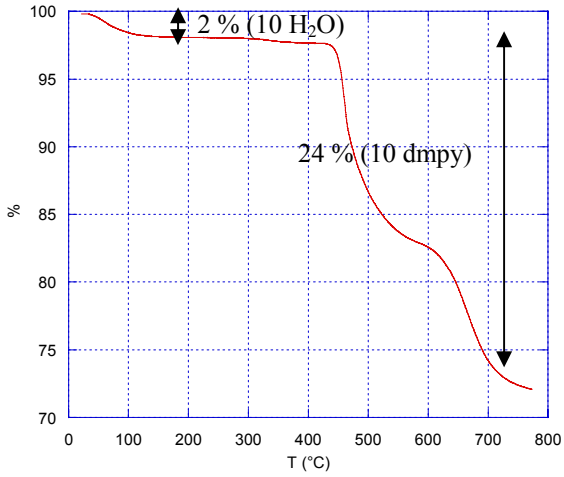

4 :

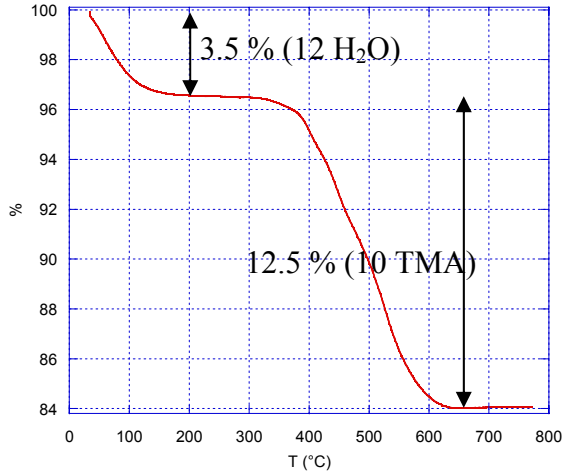

Figure SI3

Cyclic voltammograms of a 2 mM solution of $[Fe(bpy)_3](PF_6)_2$ in 0.1 M NH_4PF_6 at a bare carbon electrode (A = 0.0707 cm^2). Scan rate = 100 mV s^{-1}.